Contents list available at CBIORE journal website

International Journal of Renewable Energy Development

Journal homepage: https://ijred.cbiore.id

Research Article

Chemical characterization of activated carbon derived from Napier grass, rubber wood, bamboo, and hemp

Sarunpron Khruengsai[a], Patcharee Pripdeevech[b,c], Suwichien Pongnailert[d], Narong Chanlek[e], Kanjana Thumanu[e], Rattana Muangmora[f], Thammasak Rojviroon[f], Siwatt Pongpiachan[a,d*]

[a] *National Astronomical Research Institute of Thailand (Public Organization), Chiang Mai, Thailand*

[b] *School of Science, Mae Fah Luang University, Chiang Rai, Thailand*

[c] *Center of Chemical Innovation for Sustainability (CIS), Mae Fah Luang University, Chiang Rai, Thailand*

[d] *Graduate School of Social Development and Management Strategy, National Institute of Development Administration (NIDA), Bangkok, Thailand*

[e] *Synchrotron Light Research Institute, Nakhon Ratchasima, Thailand*

[f] *Department of Civil Engineering, Faculty of Engineering, Rajamangala University of Technology Thanyaburi, Pathum Thani, Thailand*

Abstract. This study examines the process and analysis of activated carbons that use H_2SO_4, H_2O_2, and NaOH as activating agents. The distinct chemical methods employed by each activator impacted the ash and carbon content, surface properties, and functional groups of the activated carbons, exhibiting notable disparities. The ash level varied from 6.86% to 37.08%. H_2SO_4-activated carbons had the lowest ash content, suggesting better elimination of inorganic contaminants. The iodine number, which serves as a measure of adsorption capacity, was consistent among all samples, with values ranging from 800 to 950 mg g^{-1}. This indicates that the three activating agents effectively increased the surface area and porosity. The BET surface areas varied between 9.14 and 167.42 m^2 g^{-1}, whereas the BJH adsorption surface areas ranged from 9.68 to 28.89 m^2 g^{-1}. The pore volumes ranged from 0.0071 to 0.0595 cm^2 g^{-1}, while the sizes ranged from 0.51 to 8.2 nm. These measurements suggest the presence of both micropores and mesopores. The FTIR spectra exhibited comparable functional groups among all samples, such as OH, CH, C=C, and C-O. The SEM-EDX and XPS tests showed that there was a lot of carbon. The carbon content was highest in H_2O_2-activated carbons because they were exposed to less severe oxidative conditions. These activated carbons comply with the requirements set by IUPAC and ASTM. They are suitable for catalytic processes and liquid adsorption, such as water and wastewater treatment. Subsequent research should aim to improve activation conditions to get the highest possible carbon content and optimise surface characteristics.

Keywords: Activated carbon, Adsorption capacity, Chemical activation, Elemental composition.

Received: 25th July 2024; Revised: 27th Sept 2024; Accepted: 12th Oct 2024; Available online: 17th Oct 2024

1. Introduction

Activated carbon is a porous substance that contains a high amount of carbon. It is known for its large surface area and well-defined pore structure, which includes macropores, mesopores, and micropores (Danish & Ahmad, 2018). Due to their intricate structure, these materials are well-suited for a range of applications, including as separation, purification, deodorization, decolorization, and filtering (Rengga *et al.*, 2012; Gao *et al.*, 2020). With its significant ability to adsorb, it may efficiently trap gaseous contaminants such sulfur dioxide, nitrogen oxides, tar, and carbon dioxide (Kosheleva *et al.*, 2019). They can be produced from several types of waste materials. Moreover, other inexpensive biomass products, including rice husk, coconut shells, banana peel, coffee shell, acorn shell, wood sawdust, and fruit waste, can be transformed into activated carbon (Asemave *et al.*, 2021).

Thailand, being a major player in agriculture, produces a substantial amount of biomass that can be transformed into useful products like activated carbon (Bhattacharjee *et al.*, 2021). Napier grass (*Pennisetum purpureum*) is a perennial grass that grows quickly and produces a large amount of biomass. It is commonly used as animal feed in tropical and subtropical countries. This grass has the potential to be used for making activated carbons (Prakasham *et al.*, 2014). The complex structure of Napier grass, which consists of cellulose, hemicellulose, and lignin, offers a significant amount of carbon when subjected to pyrolysis (Mohammad *et al.*, 2015). Likewise, rubberwood (*Hevea brasiliensis*), which is mostly collected for latex manufacturing, is frequently not fully exploited (Nair & Nair). Rubberwood plantations yield substantial biomass that can be transformed into valuable commodities such as activated carbon. The presence of cellulose and lignin in the biomass is essential for the formation of a porous structure during the activation process (Kumar *et al.*, 2006). Bamboo (*Bambusa vulgaris*), renowned for its fast growth and abundant biomass output, has been extensively researched for the purpose of producing activated carbon, owing to its substantial carbon

* Corresponding author
Email: siwatt.p@nida.ac.th (S. Pongpiachan)

https://doi.org/10.61435/ijred.2024.60502
ISSN: 2252-4940/© 2024.The Author(s). Published by CBIORE

content and exceptional mechanical characteristics. The distinctive composition of bamboo, which includes vascular bundles, leads to a significant increase in surface area when converted into activated carbon (Arias-Niquepa *et al.*, 2019). Hemp (*Cannabis sativa*), a rapidly growing plant with diverse uses such as textiles and biofuels, is also an ideal source for manufacturing activated carbon because of its abundant cellulose and hemicellulose content (Marrot *et al.*, 2022). The utilization of hemp for the synthesis of activated carbon not only enhances the worth of this commodity but also promotes sustainable agricultural practices (Rosas *et al.*, 2008). These biomass resources are commonly used as fuel in manufacturing processes (AliAkbari *et al.,* 2021). Nevertheless, transforming this waste into activated carbon is a more valuable option that can mitigate problems associated with disposal (AliAkbari *et al.*, 2021).

The production of activated carbons is influenced by various aspects, such as the activating agent, activation process conditions, and the characteristics of the raw material. Traditional activation procedures include both physical and chemical activation methods (Ruiz-Fernández *et al.*, 2011; Su *et al.*, 2024). Physical activation is the process of subjecting materials to elevated temperatures to induce porosity and produce different pore sizes on the surface of activated carbons (Heidarinejad *et al.*, 2020). Chemical activation, in contrast, entails saturating raw materials with chemical substances that break down cellulose, hemicellulose, and lignin. This process efficiently eliminates tar or volatile components from the material, leading to a rise in surface area and porosity (Panwar & Pawar, 2020). While physical activation does not involve the use of chemical reagents and is a less complex thermal process, it does require greater temperatures (Ruiz-Fernández *et al.,* 2011; Su *et al.,* 2024). Chemical activation is commonly favored because of its benefits, such as reduced temperatures and larger pore size. However, it does necessitate a washing procedure to eliminate any residual chemicals present in the activated carbons (Heidarinejad *et al.,* 2020). Potassium hydroxide (KOH), sodium hydroxide (NaOH), phosphoric acid (H_3PO_4), and zinc chloride ($ZnCl_2$) are among the chemical reagents that can be utilized as activating agents in chemical activation (Heidarinejad *et al.,* 2020; Mbarki *et al.,* 2022). These chemicals induce the creation of pores in activated carbons by promoting degradation and dehydration (Karapınar, 2022).

This research seeks to examine the properties of activated carbons produced from Napier grass, rubberwood, bamboo, and hemp. The focus will be on the level of microporosity, utilizing sulfuric acid (H_2SO_4), hydrogen peroxide (H_2O_2), and sodium hydroxide (NaOH) as activating agents. The aims of this study are assessing the qualities of the activated carbons produced and analyzing their surface area and pore characteristics. This research aims to improve the comprehension of the production and characteristics of activated carbon derived from biomass sources. The findings may potentially contribute to the development of more sustainable and economically feasible methods for utilizing biomass and controlling pollution.

2. Material and method

2.1. Material and Preparation of Activated Carbons

The Napier grass, rubberwood and bamboo, and hemp leaves used in this study were sourced from Pak Chong District, Nakhon Ratchasima Province, Waritchaphum District, Sakon Nakhon Province, Phang Khon District, Sakon Nakhon Province, and Mae Sot District, Tak Province, Thailand, respectively. Napier grass chips are greenish-yellow, thin, and brittle, prepared by cutting stalks into 1-2 cm lengths. Rubberwood chips, light brown and fibrous, resemble small wood flakes and are 2-3 cm long. Bamboo chips, tan-colored with a smooth texture, are sliced into thin rectangular pieces of 1-2 cm length and 0.5 cm thickness, maintaining the stalk's structure. Hemp chips, grayish-brown and lightweight, are 1-2 cm segments from shredded stalks, characterized by their high porosity and reactivity during activation. The particles were further cleaned and dried at 105 °C overnight prior storing in plastic bag avoid moisture absorption (Wang *et al.*, 2021). The average moisture content of the raw materials after drying was determined to be 5.3% for Napier grass, 6.1% for rubberwood, 4.7% for bamboo, and 5.8% for hemp leaves. The moisture content is calculated by equation 1.

$$Moisture\ Content\ (\%) = \left[\frac{Initial\ weight - Dried\ weight}{Initial\ weight}\right] \times 100 \quad (1)$$

Where initial weight is the weight of the sample before drying and dried weight is the weight of the sample after drying at 105°C until a constant weight is achieved.

For the carbonization process, a 4-inch diameter, 400 mm long electric tube furnace was employed. The precursor particles underwent carbonization at 400 °C under a nitrogen gas atmosphere for 1 h. The resulting biochar samples were collected and stored in a silica gel box to prevent moisture uptake.

The activation process utilized three different chemical agents including H_2SO_4, H_2O_2, and NaOH. The summarized activation methods for all samples are listed in Table 1. For H_2SO_4 activation, 100 g of dried biochar was mixed with 500 mL of 5 M H_2SO_4 and heated at 80 °C for 3 h. After heating, the

Table 1
Chemical activation and modification stages of activated carbons from Napier grass, rubberwood, bamboo, and hemp leaves

No.	Sample code	Treatment	
		Chemical	Temperature
1	NP-H_2SO_4	5 M H_2SO_4 80 °C 3 h	105 °C 24 h
2	RB-H_2SO_4		
3	BB-H_2SO_4		
4	H-H_2SO_4		
5	NP-H_2O_2	10 M H_2O_2 25 °C 3 h	105 °C 24 h
6	RB-H_2O_2		
7	BB-H_2O_2		
8	H-H_2O_2		
9	NP-NaOH	5 M NaOH 80 °C 3 h	105 °C 24 h
10	RB-NaOH		
11	BB-NaOH		
12	H-NaOH		

Napier grass: NP, Rubberwood: RB, Bamboo: BB, Hemp leaves: H

samples were thoroughly washed with 5 L of deionized (DI) water to neutralize the residual acid and achieve a final pH of 7. The biochar was then dried at 105 °C for 24 h. For H_2O_2 activation, 100 g of sample was treated with 10 M H_2O_2 (500 mL). This exothermic reaction, carried out in a fume hood for 3 h, raised the temperature to 80-100 °C. After the reaction, the biochar was washed with 5 L of DI water to a final pH of 7 and dried at 105 °C for 24 h. For NaOH activation, 100 g of dried biochar was mixed with 5 M NaOH (500 mL) and heated at 80 °C for 3 h. After heating, samples were washed with 5 L of DI water. A final pH of 13-14 was achieved prior drying at 105 °C for 24 h.

2.2. Characterization of Activated Carbon

2.2.1. Ash Content

The analysis of ash content was performed following the modified method of Heidarinejad *et al.* (2020). A precise amount of activated carbon sample (1.0 g) was placed in a porcelain crucible. This crucible was then placed in an oven setting temperature of 115 °C for 4 h. After this initial heating, the samples were weighed and then transferred to a muffle furnace, where they were subjected to a temperature of 800 °C for 2 h. Following this high-temperature treatment, the crucibles were removed from the furnace and placed in desiccator before weighing. The ash content was calculated using the formula:

$$Ash\ Content\ (\%) \quad = \quad \left[\frac{C-D}{C-B}\right] \times 100 \qquad (2)$$

Where B represents the weight of the crucible in grams (g), C denotes the weight of the crucible along with the sample in grams (g), and D refers to the weight of the crucible after the weight loss in grams (g).

2.2.2. Iodine Number

The value of the iodine number represents the adsorption capacity based on its porosity. It was measured using the titration method with a sodium thiosulfate solution (Saka, 2012). The formula used is as follows:

$$\frac{X}{M} \quad = \quad \left[(N_I \times 126.93 \times V_I) - \left[\frac{V_I + V_{HCl}}{V_F}\right] \times \left[\frac{N_{Na_2S_2O_3} \times 126.93 \times V_{Na_2S_2O_3}}{W_{AC}}\right]\right] \quad (3)$$

Where X and M represent the amount of iodine in mg adsorbed per mass of activated carbon in grams. N_I represents the normality of the iodine solution, V_I is the volume of iodine solution added, V_{HCl} is the volume of 5% HCl added, V_F denotes the filtrate volume used in titration, $N_{Na_2S_2O_3}$ represents the normality of the sodium thiosulfate solution, $V_{Na_2S_2O_3}$ is the volume of sodium thiosulfate solution consumed and W_{AC} is the weight of activated carbon.

2.3. Surface Area Analysis

The specific surface area, average pore volume, and pore size distribution of the activated carbon samples were evaluated using adsorption isotherms and the Brunauer–Emmett–Teller (BET) equation. Analyzed utilizing the BET method, the activated carbon samples' surface area and porosity were determined. The investigation was performed utilizing nitrogen adsorption-desorption isotherms, which were measured at a temperature of 300 °C. The study was conducted using the BELSORP Data Study Software (BEL Master, Version 7.3.1.0) on the instrument. Before the examination, the activated carbon samples underwent degassing to eliminate any moisture and contaminants. The samples were subjected to vacuum heating at 300 °C for a duration of 2 h. Following the degassing process, nitrogen adsorption-desorption measurements were conducted. The BET surface area was computed using the adsorption data, whereas the pore size distribution and pore volume were obtained from the desorption isotherms. This methodology guarantees precise determination of the surface area and porosity of the activated carbon samples, offering crucial data for their possible uses. In addition, the micropore volume and total pore volume were calculated using the Dubinin-Radushkevich equation. The pore diameter and pore size distribution were determined using the Barrett–Joyner–Halenda (BJH) model. The total pore volume was expressed as the BET surface area.

2.4. Fourier-Transform Infrared (FT-IR) Spectroscopy

The chemical functional groups of activated carbon samples were characterized using a PerkinElmer Spectrum 100 FTIR Spectrometer (Connecticut, USA). Samples were prepared by finely grinding the activated carbon and mixing with KBr in a 1:10 ratio before forming pellets. FTIR spectra were recorded in the range of 4000 cm^{-1} to 400 cm^{-1} with a resolution of 4 cm^{-1}, using 32 scans to improve signal-to-noise ratio. The resulting spectra were analyzed to identify functional groups such as –OH, C=O, and aromatic C=C bonds, using Spectrum™ software for interpretation.

2.5. Scanning Electron Microscopy and Energy Dispersive X-ray (SEM-EDX) Spectroscopy

SEM was utilized to investigate the physical morphology of the activated carbon samples, while EDX spectroscopy was used in conjunction to determine the elemental composition. The sample preparation entailed affixing the activated carbon onto conductive adhesive tape, which was subsequently positioned on aluminum stubs. The conductivity was improved to avoid the accumulation of electric charge during SEM imaging when a thin layer of gold or platinum was applied to the samples using a process called sputter-coating. The SEM study yielded intricate visual representations of the activated carbon's morphology at different levels of magnification, exposing surface features, porosity, and the distribution of particle sizes. The high-resolution photos accurately depicted the fine intricacies of the surface features, providing useful insights on the physical qualities of the materials. The utilization of this imaging approach was vital in comprehending the structure and prospective functionality of the material. Similarly, EDX spectroscopy was performed to examine the elemental makeup of the activated carbon samples. This method facilitated the detection and measurement of elements found in specific regions, as well as the generation of elemental maps to visually represent the spatial arrangement of these components on the surface of the sample. The SEM-EDX study allowed for a thorough examination of the activated carbon's physical and chemical characteristics, which is crucial for assessing its possible uses.

The SEM utilized for this investigation is a Carl Zeiss Microscopy GmbH type, EVO 18, manufactured in the United Kingdom. The device provides a resolution of 3 nm, and a magnification range from 1× to 1,000,000×, enabling precise visualization of samples. The SEM functions in both high vacuum and variable pressure modes. It is equipped with detectors for secondary electrons (SE), backscattered electrons (BSE), variable pressure secondary electrons (VPSE), and energy dispersive spectroscopy (EDS). The Energy Dispersive X-ray (EDX) system, known as EDAX, is manufactured by EDAX Inc. in the United States. The EDX system encompasses a range of modes, including spectrum acquisition, quantification, point and ID analysis, elemental mapping, and

line scanning. Quorum Technologies in the U.K. offers supplementary equipment for sample preparation, such as a sputter coater, a carbon evaporation system, and a critical point dryer. This configuration enables a thorough examination of the elemental makeup and distribution in the samples.

2.6. X-ray Photoelectron Spectroscopy (XPS) Analysis

The chemical composition and surface features of the activated carbon samples were examined using XPS with PHI5000 Versa Probe II equipment from ULVAC-PHI, Japan. The device utilized a monochromatic Al K X-ray source with an energy of 1486.6 electron volts (eV) and a beam size of 100 microns for precise examination. A preliminary survey scan was conducted to obtain a comprehensive analysis of the elemental composition on the surface of the sample. The scan was performed with an energy step of 1 eV and a pass energy of 117.40 eV, enabling the identification of different elements and their corresponding binding energies. For a more comprehensive examination, we obtained high-resolution XPS spectra for specific elements. This involved utilizing a smaller energy increment of 0.1 eV and a pass energy of 46.95 eV. The thorough scanning provided accurate data on the chemical states and bonding environments of the elements present in the activated carbon samples. The thorough XPS examination yielded crucial information regarding the chemical properties and possible uses of the activated carbon, emphasizing its elemental makeup and surface chemistry.

3. Result and discussion

3.1. Selection of the Activating Agents

Three agents were employed in the preparation of activated carbon due to their individual chemical properties (Gao *et al.*, 2020). Each agent offers unique mechanisms suitable for various applications. H_2SO_4, a strong dehydrating agent, removes water from the carbon precursor, forming a highly porous structure (Gao *et al.*, 2020). It catalyzes the breakdown of cellulose, hemicellulose, and lignin in biomass, leading to the development of micro- and mesopores (Testa & Tummino, 2021). According to a study by Kumar *et al.* (2022), H_2SO_4-activated carbon from lignocellulosic biomass showed enhanced adsorption capacities due to its well-developed pore structure, with yield percentages ranging between 64.20-94.73%. H_2O_2, an oxidizing agent, promotes porosity development by breaking down organic matter and creating oxygen-containing functional groups on the carbon surface, increasing surface area and enhancing adsorption properties (Kurniawan & Lo, 2009). It is particularly effective in generating high microporosity, suitable for gas adsorption applications, with yield percentages for the H_2O_2-activated carbon samples ranging from 74.20-90.63%. A study by Huang *et al.* (2016) demonstrated that H_2O_2-activated carbon exhibited a high degree of microporosity. Additionally, NaOH, known for its ability to penetrate and enlarge the pore structure, reacts with the carbon precursor to produce a highly porous structure, enhancing surface area and pore volume (Byamba-Ochir *et al.*, 2016). NaOH activation is effective in creating mesopores and macropores, beneficial for adsorbing larger molecules and pollutants. The yield for NaOH-activated carbon samples varied between 62.05-97.44%. Hafizuddin *et al.* (2021) indicated that NaOH-activated carbon exhibited a significantly higher surface area and pore volume.

It was noted that the higher yield of activated carbon from hemp using H_2O_2 activation, as compared to acid and base activation, can be attributed to the distinct structural properties and chemical composition of hemp biomass. Hemp has a high lignin (15-20%) and cellulose (50-70%) content, which provide rigidity and resilience during chemical activation processes (Jain *et al.*, 2015). Hydrogen peroxide, a mild oxidizing agent, selectively oxidizes surface impurities and hemicellulose without extensively degrading the cellulose-lignin matrix, thereby preserving the biomass structure (Ribeiro *et al.*, 2013; Huang *et al.*, 2016). Additionally, the intrinsic porosity and presence of aromatic compounds in hemp, derived from its high lignin content, confer resistance to harsh chemical degradation, allowing H_2O_2 to enhance surface functional groups without excessive volatilization (Ribeiro *et al.*, 2013; Huang *et al.*, 2016). This stability enables a more controlled oxidation process that minimizes structural damage. As a result, the milder nature of H_2O_2 activation is better suited for preserving the structural integrity of hemp biomass, resulting in a higher yield of

Table 2
Ash content percentage, yield percentage, iodine number, BET specific surface area, pore volume, pore diameter, and BJH adsorption cumulative surface areas of activated carbons from Napier grass, rubberwood, bamboo, and hemp leaves.

Sample code	Ash content (%)	Yield (%)	Iodine number (mg g^{-1})	BET surface area (m^2 g^{-1})	BJH adsorption (m^2 g^{-1})	Pore volume (cm^2 g^{-1})	Pore diameter (nm)
NP-H_2SO_4	16.62	71.59	836.47	23.61	19.46	0.0256	4.3423
RB-H_2SO_4	6.86	92.65	833.68	55.50	11.50	0.0071	0.5079
BB-H_2SO_4	20.36	94.73	805.75	26.09	9.68	0.0053	8.2092
H-H_2SO_4	11.08	64.62	839.26	21.32	-*	0.0222	4.1756
NP-H_2O_2	17.93	74.20	872.77	21.92	18.84	0.0108	1.8577
RB-H_2O_2	21.84	88.67	850.43	10.96	9.33	0.0121	4.4025
BB-H_2O_2	34.47	90.63	856.02	43.81	9.68	0.0193	1.1747
H-H_2O_2	20.06	75.32	950.96	167.42	-	0.0595	1.4223
NP-NaOH	31.15	76.03	830.88	17.61	12.53	0.0184	4.1712
RB-NaOH	22.48	97.44	856.02	9.14	28.89	0.0089	3.5923
BB-NaOH	37.08	95.39	850.43	68.27	-	0.0242	1.4229
H-NaOH	23.12	62.05	869.98	69.81	-	0.0248	1.4228

*Samples did not exhibit BJH values due to a mismatch between the ranges of the measurement data and the *t*-data values.

activated carbon when compared to the more severe degradation caused by acid or base activations.

In addition, yield and properties of activated carbon derived from various biomass sources, such as rice husk, coconut shell, and lignocellulosic agricultural waste have been reported extensively. For example, activated carbon derived from rice husk using KOH activation typically yields around 30-35%, depending on the activation conditions (Foo & Hameed, 2012). In contrast, coconut shell-based activated carbon yields range from 40-50%, due to its higher lignin and fixed carbon content, which makes it more resistant to degradation during activation (Gan, 2021). On the other hand, biomass with lower lignin content, such as cotton stalks, often results in lower yields (25-30%) when using microwave-assisted chemical activation (Deng *et al.*, 2009). In comparison, the activated carbons in this study showed a relatively higher yield among all samples. This higher yield can be attributed to the unique structure of plant, which has a high cellulose and lignin content, providing stability and reducing excessive mass loss during the activation process. The higher retention of mass in hemp biomass when treated with H_2O_2, compared to traditional acid or base activations, suggests that the mild oxidative conditions of H_2O_2 preserve more of the initial biomass structure.

3.2. Ash Content Analysis

The ash content percentage of all activated carbon samples is summarized in Table 2. The type of chemical activator used significantly influences the ash content, which varied from 6.86% to 37.08% across all samples. Among the activators, H_2SO_4 treatment resulted in the lowest ash content, as seen in RB-H_2SO_4 (6.86%), making it suitable for high-quality applications. The ash content in activated carbons represents the residual inorganic matter remaining after the thermal decomposition of the raw material, which is influenced by the chemical composition and carbonization degree (González *et al.*, 2009). Lower ash content is desirable as it minimizes pore blockage and maximizes the surface area available for adsorption (Foo & Hameed, 2012). The effectiveness of different activators in reducing ash content is linked to their chemical behavior. H_2O_2, for instance, acts as a strong oxidizing agent, decomposing organic material into simpler compounds and releasing gases such as CO_2 (Neyens & Baeyens, 2003). Although it enhances surface area by creating oxygen-containing functional groups (Ribeiro *et al.*, 2013), H_2O_2 is less effective at removing inorganic impurities compared to H_2SO_4, contributing to higher residual ash content in H-H_2O_2 (20.06%). In contrast, H_2SO_4 is a strong dehydrating and oxidizing agent that effectively eliminates inorganic impurities by converting them into soluble sulfates, which can be easily removed during the washing process (Behera *et al.*, 2018). This explains why H_2SO_4-treated samples have the lowest ash content. Similarly, NaOH forms sodium salts and hydroxides during the activation process, which are not easily removed (Neyens & Baeyens, 2003). These residues increase the ash content, as seen in BB-NaOH (37.08%), obstructing pores and reducing the available surface area for adsorption (Foo & Hameed, 2012). The ash content also has implications for the practical applications of activated carbon. According to the International Organization for Standardization (ISO) and the American Society for Testing and Materials (ASTM), the ash content in high-quality activated carbon should generally be less than 10% (Angın *et al.*, 2013). Therefore, the RB-H_2SO_4 sample, with an ash content of 6.86%, meets the required standards and can be applied in various fields, such as water treatment and air purification.

3.3. Iodine Number Analysis

The iodine number is a critical parameter used to evaluate the adsorption capacity and microporosity of activated carbon, specifically measuring the ability of the material to adsorb iodine molecules, which reflects its surface area and pore volume (Wang *et al.*, 2021). This metric is essential for assessing the effectiveness of activated carbon in removing small organic compounds and pollutants, making it a standard method for determining its quality and suitability across various applications (Wang *et al.*, 2021). The iodine numbers of the activated carbons in this study, presented in Table 2, range from 800 to 950 mg g^{-1}, indicating similar adsorption capacities across all activating agents. This range suggests that the activation methods-H_2SO_4, H_2O_2, and NaOH-are effective in enhancing the porosity and surface area of the resulting activated carbons, making them suitable for high-adsorption applications. These values also align with ISO and ASTM standards, which recommend an iodine number between 800 and 1,100 mg g^{-1} for high-quality activated carbon (Munoz *et al.*, 2012).

H_2SO_4, a strong dehydrating agent, breaks down cellulose, hemicellulose, and lignin into simpler carbon structures, promoting the formation of a well-developed porous network (Xiong *et al.*, 2021). This process leads to the creation of micropores, which contribute to the material's high adsorption capacity. Similarly, H_2O_2 acts as an oxidizing agent, introducing oxygen-containing functional groups that enhance surface reactivity while increasing microporosity (Neyens & Baeyens, 2003; Ribeiro *et al.*, 2013). NaOH, on the other hand, decomposes the carbon surface, increasing both mesopores and macropores, which contributes to a broader pore structure and enhanced adsorption capacity (Lim *et al.*, 2024). The slight variation in iodine numbers among the samples suggests that while all activators effectively enhance microporosity, the mechanisms by which they do so differ. For instance, the highest iodine number (950.96 mg g^{-1}) was observed in hemp leaves treated with H_2O_2 (H-H_2O_2), reflecting the strong microporous structure created by the oxidative nature of H_2O_2 (Ribeiro *et al.*, 2013). In contrast, bamboo treated with H_2SO_4 (BB-H_2SO_4) showed the lowest iodine number (805.75 mg g^{-1}), likely due to the blockage of micropores by the higher ash content present in bamboo-based activated carbons (Deng *et al.*, 2009). Despite these differences, the iodine numbers across all samples fall within the recommended range, indicating their high surface area and effective adsorption capabilities, which make them suitable for applications such as water treatment and air purification.

3.4. Surface Area Analysis

The BET and BJH surface areas, along with the pore size distribution of all synthesized activated carbons, are presented in Table 2. The BET surface areas range from 9.14 to 167.42 m^2 g^{-1}, and the BJH adsorption surface areas span between 9.68 and 28.89 m^2 g^{-1} across all activation treatments. Similarly, the pore volumes and diameters vary from 0.0071 to 0.0595 cm^3 g^{-1} and 0.5079 to 8.2092 nm, respectively, indicating a mix of micropores and mesopores in the resulting activated carbons. According to IUPAC and ASTM standards, high-quality activated carbons typically exhibit BET surface areas in the range of 500 to 1500 m^2 g^{-1} and mesopore surface areas (BJH) of 50 to 200 m^2 g^{-1}, which are crucial for effective adsorption and catalytic applications (Saka, 2012). The relatively low BET and BJH surface areas observed in this study suggest that further optimization of activation conditions is required to achieve the desired textural properties. The classification of pore sizes according to IUPAC standards distinguishes

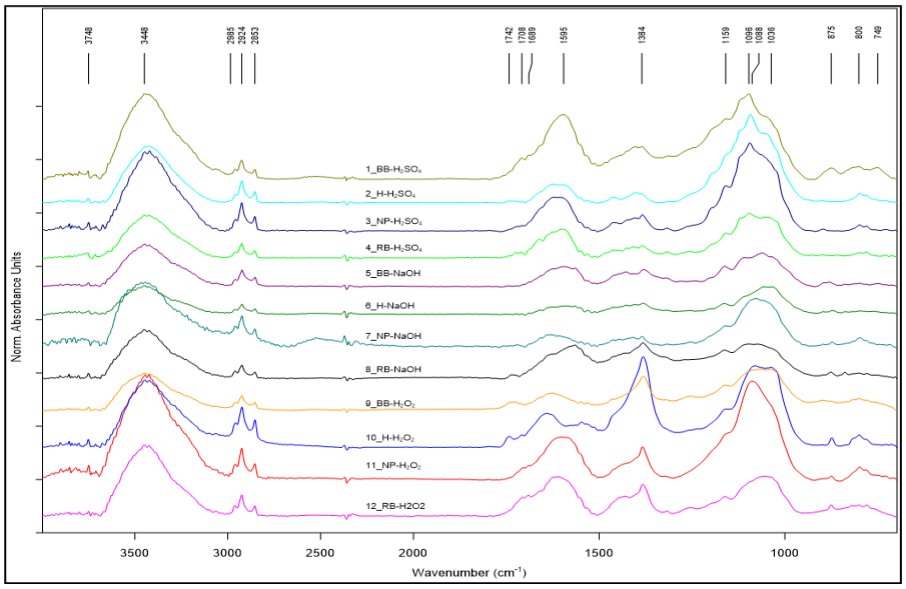

Fig. 1 FTIR spectra of all activated carbons from Napier grass, rubberwood, bamboo, and hemp leaves.

micropores (diameter < 2 nm), mesopores (2-50 nm), and macropores (diameter > 50 nm) (Bashkova *et al.*, 2009). Micropores are primarily responsible for gas adsorption due to their high surface area and small size, while mesopores are more suitable for liquid-phase adsorption because they facilitate the diffusion of larger molecules (Ribeiro *et al.*, 2013). In this study, Napier grass treated with H_2SO_4 (NP-H_2SO_4) exhibited the largest pore diameter at 4.342 nm, while rubberwood treated with H_2SO_4 (RB-H_2SO_4) had the smallest pore diameter at 0.5079 nm, indicating differences in pore development based on the chemical structure of the raw materials and activation method used (Foo & Hameed, 2011).

The BET surface area of hemp-based activated carbon treated with H_2O_2 (H-H_2O_2) reached 167.42 m^2 g^{-1}, the highest among the samples, suggesting that H_2O_2 promotes significant micropore formation in hemp, likely due to its ability to create oxygen-containing functional groups that enhance pore development (Contescu *et al.*, 2018). Conversely, the lowest BET surface area was found in rubberwood treated with H_2O_2 (RB-H_2O_2) at 10.96 m^2 g^{-1}, which may be due to the denser, more crystalline cellulose structure of rubberwood, making it less responsive to oxidative activation. Similarly, bamboo activated with NaOH (BB-NaOH) had the highest BJH adsorption surface area (68.27 m^2 g^{-1}), indicating extensive mesopore development, which is beneficial for applications like dye removal and liquid-phase adsorption (Huang *et al.*, 2016). However, the relatively low BJH values observed in other samples, such as H-H_2SO_4, suggest limitations in mesopore development, likely due to the interference of high ash content, which obstructs pore formation (Deng *et al.*, 2009). These results highlight the need to optimize key activation parameters, including temperature, activation time, and chemical concentration, to enhance the surface area and porosity of the synthesized activated carbons (Angın *et al.*, 2013; Lim *et al.*, 2024). By tailoring these conditions, it may be possible to achieve BET surface areas and mesopore volumes that meet the recommended standards for high-performance adsorption and catalysis applications.

3.5. FT-IR Analysis

The functional groups of all activated carbons from three different agents are shown in Fig. 1. The FTIR spectra of activated carbons derived from all activators reveal similar functional groups and structural characteristics, providing similar surface chemistry and potential applications. The FTIR spectrum of H_2SO_4 and NaOH-activated carbons typically shows broad absorption bands around 3,400 cm^{-1}, indicating the presence of hydroxyl (OH) groups due to hydration during activation. Peaks around 3,000 cm^{-1} correspond to CH stretching vibrations from alkyl groups. Additionally, peaks range 1,650-1,540 cm^{-1} representing C=C stretching while 1,230-976 cm^{-1} indicates the presence of C-O stretching. The FTIR spectrum indicating the presence of OH, CH, C=C, and C-O functional groups suggests that H_2SO_4 and NaOH-activated carbons have a diverse range of active sites, making them versatile adsorbents for various applications such as water purification, wastewater treatment, and the removal of organic and aromatic pollutants.

The FTIR spectrum of H_2O_2-activated carbon displays broad bands around 3,400 cm^{-1} and 3,000 cm^{-1}, suggesting the presence of hydroxyl (OH) groups and CH Stretching. Peaks range 1,500-1,350 cm^{-1} due to C=C stretching. Peaks around 1,300 cm^{-1} and 1,100 cm^{-1} indicate CH bending and C-O stretching, respectively. The CH bending detected in activated carbons from H_2O_2 enhances the adsorption of non-polar compounds through hydrophobic interactions, it may slightly reduce the adsorption efficiency for polar compounds. However, the effectiveness will depend on the specific contaminants present, and the potential for selective adsorption should be considered when determining the suitability for a particular application. Overall, the described FTIR characteristics indicate good potential for a wide range of adsorption applications.

3.6. Elemental Composition Analysis

The SEM images of all activated carbons are shown in Fig. 2. The external surface was quite irregular shape with rough surface because of the grinding treatment. No pores were detected within these micrographs among all samples.

In the SEM-EDX and XPS analysis, the relative percentage of all elements in activated carbons was analyzed, as shown in Table 3 and Table 4, respectively. These results show that most samples contained a high relative percentage of carbon. The carbon content in the activated carbons from H_2O_2 activator was higher than those obtained from other agents. Activated carbons from H_2SO_4 and NaOH also showed the presence of sulfur and sodium resulting by the impurity of chemical during

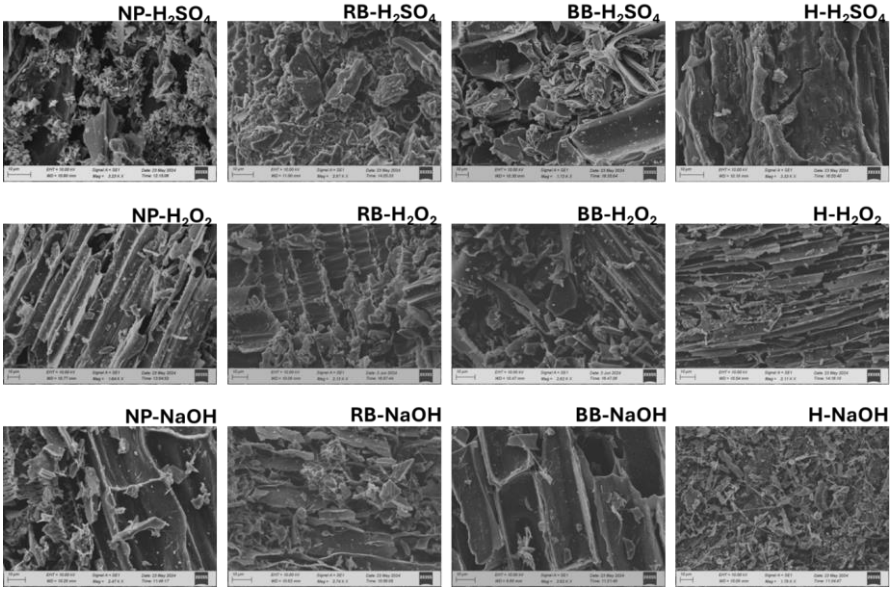

Fig. 2 SEM images of activated carbons from Napier grass, rubberwood, bamboo, and hemp leaves obtained from various treatments in Table 1 at a magnification of 1×5,000.

Table 3
Relative percentage of elements in activated carbons from Napier grass, rubberwood, bamboo, and hemp leaves obtained from SEM-EDX technique

Sample code	Relative weight (%)												
	C	O	Mg	Al	Na	Si	P	S	K	Ca	Cl	Pd	Tm
NP-H_2SO_4	20.12	43.88	1.03	2.31		3.31	1.79	18.84	8.72				
RB-H_2SO_4	45.37	30.35				1.27		19.97		3.05			
BB-H_2SO_4	64.90	21.06					3.21	7.12	3.71				
H-H_2SO_4	63.74	20.92				1.47		12.11	1.77				
NP-H_2O_2	75.33	15.43	1.60			1.95			3.78		1.92		
RB-H_2O_2	78.46	21.54											
BB-H_2O_2	69.86	15.58	1.67			3.63			9.25				
H-H_2O_2	77.37	14.56	1.60			2.51			3.97				
NP-NaOH	46.23	24.22	2.14		11.10	16.31							
RB-NaOH	56.79	25.71			17.50								
BB-NaOH	72.48	19.95			7.58								
H-NaOH	25.84	29.08	1.30		13.27		6.12		2.19	13.61		3.53	5.06

C: Carbon, O: Oxygen, Mg: Magnesium, Al: Aluminium, Na: Sodium, Si: Silicon, P: Phosphorus, S: Sulphur, K: potassium, Ca: Calcium, Cl: Chlorine, Pd: Palladium, Tm: Thulium

impregnation (Bashkova *et al.*, 2009; Angın *et al.*, 2013; Lim *et al.*, 2024). In addition, other elements such as magnesium, silicon, phosphorus potassium, and calcium were also found in activated carbons. This may be the contaminants in the raw materials. The higher carbon content in H_2O_2-activated carbons is attributed to the milder oxidative conditions provided by H_2O_2, which effectively removes volatiles while preserving the carbon framework (Jalilian *et al.*, 2024). In contrast, the more aggressive dehydration involved in H_2SO_4 and NaOH activation led to greater carbon loss and incorporation of non-carbon elements, resulting in lower overall carbon content.

The carbon content of our activated carbon samples ranges from 20% to 80%, which is significantly below the recommended standards set by IUPAC and ASTM (Wang *et al.*, 2017). These standards generally suggest that high-quality activated carbon should have a carbon content exceeding 80%, often reaching 85-90%, to ensure optimal adsorption properties and minimal impurities. Activated carbons with carbon content below 80% are likely to exhibit reduced adsorption capacities due to the fewer available adsorption sites. This limits their effectiveness in applications such as water and air purification, where high adsorption efficiency is crucial. Moreover, lower carbon content often correlates with higher levels of inorganic impurities (ash content), which can clog the pores of the activated carbon and interfere with its performance. High ash content can also introduce unwanted chemical reactions during the adsorption process, further diminishing the efficacy of the activated carbon (Neyens & Baeyens, 2003; González *et al.*, 2009; Ribeiro *et al.*, 2013). The structural integrity and mechanical strength of activated carbon are also influenced by

Table 4
Relative percentage of elements in activated carbons from Napier grass, rubberwood, bamboo, and hemp leaves obtained from XPS technique.

Sample code	% relative element								
	C	O	N	S	Si	Mg	Na	P	Ca
NP-H_2SO_4	23.31	59.80	2.51	2.66	11.71				
RB-H_2SO_4	54.80	33.46	5.14	6.60					
BB-H_2SO_4	59.08	29.75	5.09	5.14				0.94	
H-H_2SO_4	65.91	26.67	2.87	2.89	1.65				
NP-H_2O_2	74.79	21.64			2.24	1.32			
RB-H_2O_2	78.52	19.16			2.32				
BB-H_2O_2	81.60	16.33			2.07				
H-H_2O_2	72.43	22.91			0.71	0.97			2.98
NP-NaOH	56.51	30.69			6.18		4.14		2.48
RB-NaOH	59.50	26.28					14.22		
BB-NaOH	75.84	18.80			2.86		2.49		
H-NaOH	68.33	24.17			1.19	1.17	3.95		1.18

C: Carbon, O: Oxygen, N: Nitrogen, S: Sulphur, Si: Silicon, Mg: Magnesium, Na: Sodium, P: Phosphorus, Ca: Calcium

its carbon content. Lower carbon content may result in a weaker carbon matrix, reducing the durability and lifespan of the activated carbon in practical applications (Jalilian *et al.*, 2024). This can be particularly problematic in industrial processes where robust materials are required to withstand harsh conditions. The low carbon content observed in our samples may be attributed to the activation process, including the type of activating agent, temperature, and duration (Wang *et al.*, 2017). Optimizing these parameters can enhance the carbonization process, driving off more volatile components and increasing the carbon content (Wang *et al.*, 2017). Additionally, the quality and type of raw material used for producing activated carbon significantly impacts the final carbon content. Using high-carbon precursors and ensuring proper preprocessing steps, such as drying and size reduction, can improve the carbon yield.

4. Conclusions

This study investigated the preparation and characterization of activated carbons using H_2SO_4, H_2O_2, and NaOH as activating agents. The results showed significant differences in ash and carbon content, surface characteristics, and functional groups due to the distinct chemical mechanisms of each activator. H_2SO_4-activated carbons showed the lowest ash content, indicating efficient impurity removal. The iodine number was similar across all samples, suggesting effective enhancement of surface area and porosity by all activators. BET surface areas ranged from 9.14 to 167.42 $m^2\ g^{-1}$, while BJH adsorption surface areas ranged from 9.68 to 28.89 $m^2\ g^{-1}$. Pore volumes and diameters varied, indicating a mix of micropores and mesopores. FTIR spectra revealed similar functional groups across all samples, including OH, CH, C=C, and C-O groups. SEM-EDX and XPS analyses showed a high carbon content, with H_2O_2-activated carbons having the highest due to milder oxidative conditions. These activated carbons meet IUPAC and ASTM standards, making them suitable for catalytic processes and liquid-phase adsorption, including water and wastewater treatment. Future work should optimize activation conditions to maximize carbon content and surface properties.

Acknowledgement

We would like to extend our heartfelt gratitude to all the staff members of the Synchrotron Light Research Institute for their invaluable contributions to the chemical analysis. Your expertise and dedication have been instrumental in advancing our research. Additionally, we are deeply grateful to the staff of Rajamangala University of Technology Thanyaburi for their tireless efforts in generating the activated carbon samples. Your hard work and commitment have significantly supported our project. Thank you for your unwavering support and exceptional work.

References

AliAkbari, R., Ghasemi, M. H., Neekzad, N., Kowsari, E., Ramakrishna, S., Mehrali, M., & Marfavi, Y. (2021). High value add bio-based low-carbon materials: conversion processes and circular economy. *Journal of Cleaner Production*, 293, 126101. https://doi.org/10.1016/j.jclepro.2021.126101

Angın, D., Altintig, E., & Köse, T. E. (2013). Influence of process parameters on the surface and chemical properties of activated carbon obtained from biochar by chemical activation. *Bioresource Technology*, 148, 542-549. https://doi.org/10.1016/j.biortech.2013.08.164

Arias-Niquepa, R. A., Prías-Barragán, J. J., Ariza-Calderón, H., & Rodríguez-García, M. E. (2019). Activated carbon obtained from bamboo: Synthesis, morphological, vibrational, and electrical properties and possible temperature sensor. *Physica Status Solidi (a)*, 216(4), 1800422. https://doi.org/10.1002/pssa.201800422

Asemave, K., Thaddeus, L., & Tarhemba, P. T. (2021). Lignocellulosic-based sorbents: a review. *Sustainable Chemistry*, 2(2), 271-285. https://doi.org/10.3390/suschem2020016

Bashkova, S., Armstrong, T. R., & Schwartz, V. (2009). Selective catalytic oxidation of hydrogen sulfide on activated carbons impregnated with sodium hydroxide. *Energy & Fuels*, 23(3), 1674-1682. https://doi.org/10.1021/ef800711c

Behera, S. K., Kumari, U., & Meikap, B. C. (2018). A review of chemical leaching of coal by acid and alkali solution. *Journal of Mining and Metallurgy A: Mining*, 54(1), 1-24.

Bergna, D., Varila, T., Romar, H., & Lassi, U. (2018). Comparison of the properties of activated carbons produced in one-stage and two-stage processes. *C*, 4(3), 41. https://doi.org/10.3390/c4030041.

Bhattacharjee, A., Bhowmik, M., Paul, C., Chowdhury, B. D., & Debnath, B. (2021). Rubber tree seed utilization for green energy, revenue generation and sustainable development–A comprehensive review. *Industrial Crops and Products*, 174, 114186. https://doi.org/10.1016/j.indcrop.2021.114186

Byamba-Ochir, N., Shim, W. G., Balathanigaimani, M. S., & Moon, H. (2016). Highly porous activated carbons prepared from carbon rich Mongolian anthracite by direct NaOH activation. *Applied Surface Science*, 379, 331-337. https://doi.org/10.1016/j.apsusc.2016.04.082

Contescu, C. I., Adhikari, S. P., Gallego, N. C., Evans, N. D., & Biss, B. E. (2018). Activated carbons derived from high-temperature pyrolysis of lignocellulosic biomass. *C*, 4(3), 51. https://doi.org/10.3390/c4030051.

Danish, M., & Ahmad, T. (2018). A review on utilization of wood biomass as a sustainable precursor for activated carbon production and application. *Renewable and Sustainable Energy Reviews*, 87, 1-21. https://doi.org/10.1016/j.rser.2018.02.003

Deng, H., Yang, L., Tao, G., & Dai, J. (2009). Preparation and characterization of activated carbon from cotton stalk by microwave-assisted chemical activation—application in methylene blue adsorption from aqueous solution. *Journal of Hazardous Materials*, 166(2–3), 1514–1521. https://doi.org/10.1016/j.jhazmat.2008.12.043.

Foo, K. Y., & Hameed, B. H. (2011). Microwave-assisted preparation of oil palm fiber activated carbon for methylene blue adsorption. Chemical Engineering Journal, 166(2), 792–795. https://doi.org/10.1016/j.cej.2010.11.004.

Foo, K. Y., & Hameed, B. H. (2012). Utilization of rice husks as a feedstock for preparation of activated carbon by microwave induced KOH and K_2CO_3 activation. *Bioresource Technology*, 102(20), 9814-9817. https://doi.org/10.1016/j.biortech.2011.11.026.

Gan, Y. X. (2021). Activated Carbon from Biomass Sustainable Sources. *Carbon Letters*, 7(2), 39. https://doi.org/10.3390/c7020039.

Gao, Y., Yue, Q., Gao, B., & Li, A. (2020). Insight into activated carbon from different kinds of chemical activating agents: A review. *Science of the Total Environment*, 746, 141094. https://doi.org/10.1016/j.scitotenv.2020.141094

González, J. F., Román, S., Encinar, J. M., & Martínez, G. (2009). Pyrolysis of various biomass residues and char utilization for the production of activated carbons. *Journal of Analytical and Applied Pyrolysis*, 85(1-2), 134-141. https://doi.org/10.1016/j.jaap.2008.11.035

Hafizuddin, M. S., Lee, C. L., Chin, K. L., H'ng, P. S., Khoo, P. S., & Rashid, U. (2021). Fabrication of highly microporous structure activated carbon via surface modification with sodium hydroxide. *Polymers*, 13(22), 3954. https://doi.org/10.3390/polym13223954

Heidarinejad, Z., Dehghani, M. H., Heidari, M., Javedan, G., Ali, I., & Sillanpää, M. (2020). Methods for preparation and activation of activated carbon: a review. *Environmental Chemistry Letters*, 18, 393-415. https://doi.org/10.1007/s10311-019-00955-0

Huang, D., Wang, Y., Zhang, C., Zeng, G., Lai, C., Wan, J., Gin, L. & Zeng, Y. (2016). Influence of morphological and chemical features of biochar on hydrogen peroxide activation: implications on sulfamethazine degradation. *RSC Advances*, 6(77), 73186-73196. https://doi.org/10.1039/C6RA11850J

Jain, A., Balasubramanian, R., & Srinivasan, M. P. (2015). Production of high surface area mesoporous activated carbons from waste biomass using hydrogen peroxide-mediated hydrothermal treatment for adsorption applications. *Chemical Engineering Journal*, 273, 622-629. https://doi.org/10.1016/j.cej.2015.03.111

Jalilian, M., Bissessur, R., Ahmed, M., Hsiao, A., He, Q. S., & Hu, Y. (2024). A review: Hydrochar as potential adsorbents for wastewater treatment and CO_2 adsorption. *Science of The Total Environment*, 169823. https://doi.org/10.1016/j.scitotenv.2023.169823

Karapınar, H. S. (2022). Adsorption performance of activated carbon synthesis by ZnCl2, KOH, H3PO4 with different activation temperatures from mixed fruit seeds. *Environmental Technology*, 43(9), 1417-1435. https://doi.org/10.1080/09593330.2021.1968507

Kosheleva, R. I., Kyzas, G. Z., & Mitropoulos, A. C. (2019). Low-cost materials in gas-phase adsorption. *In Interface Science and Technology*, 30, 125-149. https://doi.org/10.1016/B978-0-12-814178-6.00006-6

Kumar, B. P., Shivakamy, K., Miranda, L. R., & Velan, M. (2006). Preparation of steam activated carbon from rubberwood sawdust (Hevea brasiliensis) and its adsorption kinetics. *Journal of Hazardous Materials*, 136(3), 922-929. https://doi.org/10.1016/j.jhazmat.2006.01.037

Kumar, N., Kim, S. B., Lee, S. Y., & Park, S. J. (2022). Recent advanced supercapacitor: a review of storage mechanisms, electrode materials, modification, and perspectives. *Nanomaterials*, 12(20), 3708. https://doi.org/10.3390/nano12203708

Kurniawan, T. A., & Lo, W. H. (2009). Removal of refractory compounds from stabilized landfill leachate using an integrated H_2O_2 oxidation and granular activated carbon (GAC) adsorption treatment. *Water Research*, 43(16), 4079-4091. https://doi.org/10.1016/j.watres.2009.06.060

Lim, M. S., Kang, S. H., Song, D. Y., Chae, J. S., Lee, J. W., Lee, Y., & Roh, K. C. (2024). Tailoring mesoporous and macroporous structures in activated carbon from NaOH-pretreated oak for superior supercapacitors. *Journal of Energy Storage*, 96, 112729. https://doi.org/10.1016/j.est.2024.112729

Marrot, L., Candelier, K., Valette, J., Lanvin, C., Horvat, B., Legan, L., & DeVallance, D. B. (2022). Valorization of hemp stalk waste through thermochemical conversion for energy and electrical applications. *Waste and Biomass Valorization*, 1-19. https://doi.org/10.1007/s12649-021-01640-6

Mbarki, F., Selmi, T., Kesraoui, A., & Seffen, M. (2022). Low-cost activated carbon preparation from Corn stigmata fibers chemically activated using H3PO4, ZnCl2 and KOH: Study of methylene blue adsorption, stochastic isotherm and fractal kinetic. *Industrial Crops and Products*, 178, 114546. https://doi.org/10.1016/j.indcrop.2022.114546

Mohammad, I., Abakr, Y., Kabir, F., Yusuf, S., Alshareef, I., & Chin, S. (2015). Pyrolysis of Napier grass in a fixed bed reactor: effect of operating conditions on product yields and characteristics. *BioResources*, 10(4), 6457-6478. https://orcid.org/0000-0002-3121-9086

Munoz, R. A., Fernandes, D. M., Santos, D. Q., Barbosa, T. G., & Sousa, R. M. (2012). Biodiesel: production, characterization, metallic corrosion and analytical methods for contaminants. *Biodiesel-Feedstocks, Production and Applications*, 3, 48. https://doi.org/10.5772/53655

Nair, K. P., & Nair, K. P. (2021). Rubber (*Hevea brasiliensis*). Tree Crops: Harvesting cash from the world's important cash crops, 287-332. https://doi.org/10.1007/978-3-030-62140-7_8

Neyens, E., & Baeyens, J. (2003). A review of classic Fenton's peroxidation as an advanced oxidation technique. *Journal of Hazardous Materials*, 98(1-3), 33-50. https://doi.org/10.1016/S0304-3894(02)00282-0

Panwar, N. L., & Pawar, A. (2020). Influence of activation conditions on the physicochemical properties of activated biochar: A review. *Biomass Conversion and Biorefinery*, 1-23. https://doi.org/10.1007/s13399-020-00870-3

Prakasham, R. S., Nagaiah, D., Vinutha, K. S., Uma, A., Chiranjeevi, T., Umakanth, A. V., Rao, P. S. & Yan, N. (2014). Sorghum biomass: a novel renewable carbon source for industrial bioproducts. *Biofuels*, 5(2), 159-174. https://doi.org/10.4155/bfs.13.74

Rengga, W. D. P., Sudibandriyo, M., & Nasikin, M. (2012). Development of formaldehyde adsorption using modified activated carbon–A review. *International Journal of Renewable Energy Development*, 1(3), 75-80. https://doi.org/10.14710/ijred.1.3.75-80

Ribeiro, R. S., Silva, A. M., Figueiredo, J. L., Faria, J. L., & Gomes, H. T. (2013). The influence of structure and surface chemistry of carbon materials on the decomposition of hydrogen peroxide. *Carbon*, 62, 97-108. https://doi.org/10.1016/j.carbon.2013.06.001

Rosas, J. M., Bedia, J., Rodríguez-Mirasol, J., & Cordero, T. (2008). Preparation of hemp-derived activated carbon monoliths.

Adsorption of water vapor. *Industrial & Engineering Chemistry Research*, 47(4), 1288-1296. https://doi.org/10.1021/ie070924w

Ruiz-Fernández, M., Alexandre-Franco, M., Fernández-González, C., & Gómez-Serrano, V. (2011). Development of activated carbon from vine shoots by physical and chemical activation methods. Some insight into activation mechanisms. *Adsorption*, 17, 621-629. https://doi.org/10.1007/s10450-011-9347-1

Saka, C. (2012). BET, TG–DTG, FT-IR, SEM, iodine number analysis and preparation of activated carbon from acorn shell by chemical activation with $ZnCl_2$. *Journal of Analytical and Applied Pyrolysis*, 95, 21-24. https://doi.org/10.1016/j.jaap.2011.12.020

Su, X., Ren, Z., & Li, P. (2024). Review on physical and chemical activation strategies for ultra-high performance concrete (UHPC). *Cement and Concrete Composites*, 105519. https://doi.org/10.1016/j.cemconcomp.2024.105519

Testa, M. L., & Tummino, M. L. (2021). Lignocellulose biomass as a multifunctional tool for sustainable catalysis and chemicals: an overview. *Catalysts*, 11, 125. https://doi.org/10.3390/catal11010125

Wang, H., Xu, J., Liu, X., & Sheng, L. (2021). Preparation of straw activated carbon and its application in wastewater treatment: A review. *Journal of Cleaner Production*, 283, 124671. https://doi.org/10.1016/j.jclepro.2020.124671

Wang, J., Liu, T. L., Huang, Q. X., Ma, Z. Y., Chi, Y., & Yan, J. H. (2017). Production and characterization of high quality activated carbon from oily sludge. *Fuel Processing Technology*, 162, 13-19. https://doi.org/10.1016/j.fuproc.2017.03.017

Xiong, S., Guan, Y., Luo, C., Zhu, L., & Wang, S. (2021). Critical review on the preparation of platform compounds from biomass or saccharides via hydrothermal conversion over carbon-based solid acid catalysts. *Energy & Fuels*, 35(18), 14462-14483. https://doi.org/10.1021/acs.energyfuels.1c02672